ELSEVIER

Journal of Power Sources 87 (2000) 57–63

JOURNAL OF POWER SOURCES

www.elsevier.com/locate/jpowsour

Modelling of gas transport phenomena in SOFC anodes

W. Lehnert [1], J. Meusinger [1], F. Thom *

Institute of Energy Process Engineering, Forschungszentrum Jülich, 52425 Jülich, Germany

Received 15 June 1999; received in revised form 19 August 1999; accepted 19 August 1999

Abstract

Internal steam reforming in SOFC cells leads to inhomogeneous temperature distributions according to the fast reforming reaction kinetics. This results in thermal induced stresses and may lead therefor to mechanical failure of the material. A one-dimensional numerical simulation program has been developed to describe the transport of gases inside the SOFC anode due to diffusion and permeation as well as the kinetic of the reforming reaction and the electrochemistry. Simulations with experimentally determined reaction rates and structural properties of the anode materials have been performed. In order to reduce the methane conversion rate, a sensitivity analysis has been performed. It can be shown, e.g., that a reduction of the structural parameter ψ which is the ratio of porosity ε to tortuosity δ of 26.28% compared to standard material leads to a lowering of the methane conversion rate of 12.24%. Finally, produced cermets are screened in view of a conversion lowering effect.

Keywords: SOFC; Anode; Structural parameter; Numerical simulation; Diffusion; Reforming kinetics

1. Introduction

The operating temperature of solid oxide fuel cells (SOFC) is about 950°C. Because of the high operating temperature this type of fuel cell will be most suitable for stationary applications like power plants in the range of kW up to MW. One advantage of solid oxide fuel cells compared to low temperature fuel cells is that they cannot only convert hydrogen into electricity, but also carbon monoxide. Furthermore, the fuel cell can be fed with methane. Due to the high temperature, the methane can be converted to H_2 and CO in a steam reforming process within the cell. This reforming process takes place at the surface of the anode material which is typically a porous nickel cermet (ceramic metal). The catalytic active Ni is implemented in yttrium (8 mol% Y_2O_3) stabilized zirconia (ZrO_2).

The methane reforming reaction scheme can be formulated as follows (I)

$$CH_4 + H_2O \rightleftarrows 3H_2 + CO \quad \Delta H_{298} = 206\ \text{kJ/mol} \qquad \text{(I)}$$

The heat necessary to sustain the endothermic reforming process is supplied by the exothermic electrochemical reactions (Eqs. (II) and (III)):

$$H_2 + \frac{1}{2}O \rightarrow H_2O \quad \Delta H_{298} = -241\ \text{kJ/mol} \qquad \text{(II)}$$

$$CO + \frac{1}{2}O \rightarrow CO_2 \quad \Delta H_{298} = -283\ \text{kJ/mol} \qquad \text{(III)}$$

At the Research Centre Jülich an anode supported planar substrate concept has been developed [1] consisting of thin electrolyte films (10 μm) deposited on thick anode substrates (2 mm). A schematic diagram of this concept is given in Fig. 1. The thin electrolyte allows operating temperatures in the 750 to 850°C range. Due to the lower operating temperature compared to conventional SOFCs operating at about 950–1000°C, the materials of the cells and the stacks are cheaper and also all other components of the whole system can be lowered in price.

* Corresponding author. Tel.: +49-2461-616715; e-mail: f.thom@fz-juelich.de

[1] Present address: Adam Opel, Rüsselsheim, Germany.

0378-7753/00/$ - see front matter
PII: S0378-7753(99)00356-0

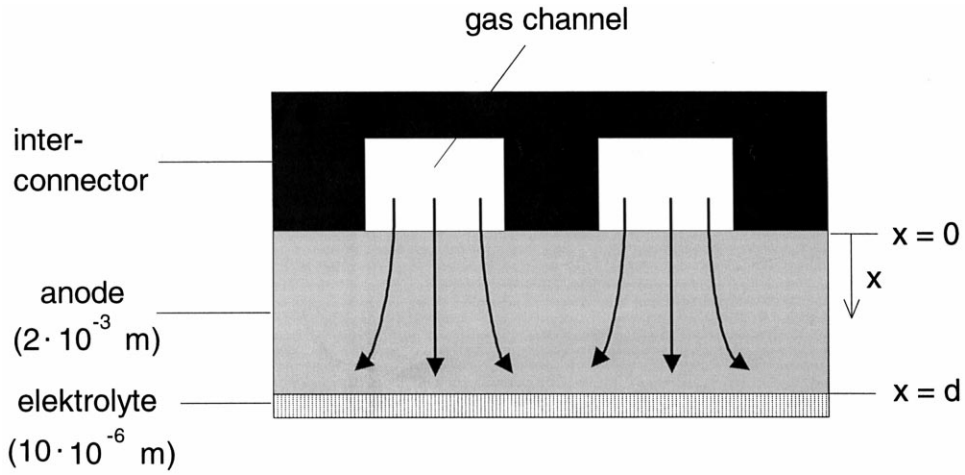

Fig. 1. Substrate concept.

However, in the entrance of the cermet, the ratio of the steam reforming reaction rate (IV) at 900°C is about 42 times higher than the reaction rate of the electrochemical processes at 300 mA/cm^2. At 700°C the ratio is still 7.2 [2]. The fast kinetics of the endothermic steam reforming reaction leads to local subcooling in this area, which may result in mechanical failure due to thermally induced stresses.

In the present study, mass transport phenomena in the porous cermet, such as diffusion and permeation, accompanied by chemical and electrochemical reactions (internal reforming and electrochemistry) are studied and the resulting model is implemented in a numerical simulation program. The knowledge about the relationship of structural properties and the reforming reactions leads to a determination of those parameters which affect the methane conversion rate mostly. Additionally, produced anode-cermets can be screened in view of lower conversion rates and accordingly reduced stresses in the entrance of the cermet.

2. Diffusion and permeation of gases through porous media

The transport process of the gases in the porous cermet structure will be described in the frame of the mean transport pore model (MTPM) [3]. This model is based on the assumption that the structure of the porous medium is isotrop so that the cermet can be described by three structural parameters taken into consideration in the diffusion and permeation equations.

- The first model parameter is ψ, which is the ratio of porosity ε to tortuosity δ. The porosity describes only those transport pores which are relevant to gas transport. Branches and hollows within the structure are not considered.
- The mean value of pore radii $\langle r \rangle$ (second model parameter): It is assumed that the gas transport takes place in pores being visualized as cylindrical capillaries.
- The third model parameter is the mean value of squared transport pore radius $\langle r^2 \rangle$.

Within the MTPM diffusion and permeation processes can be described in the following form:

$$N_i = N_i^{\mathrm{d}} + N_i^{\mathrm{p}} \left[\mathrm{mol}/(\mathrm{m}^2\mathrm{s})\right] \tag{1}$$

where the first term on the right side of the equation N_i^{d} represents the contribution according to the molar net diffusion flux density and the second term N_i^{p} the contribution according to the molar net permeation flux density. The diffusion flux (Eq. (2.1)) is based on the Stefan–Maxwell equation dealing with the molecular diffusion and is extended by the term of the Knudsen diffusion.

$$\frac{N_i^{\mathrm{d}}}{D_i^{\mathrm{k}}} + \sum_{\substack{j=1 \\ i \neq j}}^{n} \frac{y_j N_i^{\mathrm{d}} - y_i N_j^{\mathrm{d}}}{D_{ij}^{\mathrm{m}}} = -c_{\mathrm{t}} \frac{\mathrm{d}\, y_i}{\mathrm{d}\, x} \tag{2.1}$$

$i = 1, \ldots n$

with

$$D_{ij}^{\mathrm{m}} = \Psi \delta_{ij} \left[\mathrm{m}^2/\mathrm{s}\right] \tag{2.2}$$

$$D_i^{\mathrm{k}} = \Psi \langle r \rangle \frac{2}{3} \sqrt{\frac{8RT}{\pi M_i}} \left[\mathrm{m}^2/\mathrm{s}\right] \tag{2.3}$$

c_{t} is the total molar mixture concentration, y_i the mole fraction of component i and x the length in transport direction. D_{ij}^{m} denotes the effective binary diffusion coeffi-

Table 1
Textural properties of different cermet materials

Structural parameter	DS 42	Standard cermet	DS 45
ψ (–)	0.115	0.156	0.211
$\langle r \rangle$ (10^{-6} m)	0.517	1.07	2.02
$\langle r^2 \rangle$ (10^{-12} m^2)	0.18	0.38	1.53

cient in the porous structure, D_i^k the effective Knudsen diffusion coefficient and δ_{ij} is the gas–gas diffusion coefficient.

The permeation molar flux density is described by the Darcy law (Eq. (3.1)), which is valid for small Reynolds numbers:

$$N_i^p = -y_i B_i \frac{dc_t}{dx} \left[\text{mol}/(\text{m}^2\text{s})\right] \quad (3.1)$$

where B_i signifies the permeability coefficient of component i:

$$B_i = K_i \psi \langle r \rangle \phi + \omega K_i \psi \langle r \rangle (1-\phi) + \frac{\langle r^2 \rangle \psi p}{8\eta} \left[\text{m}^2/\text{s}\right] \quad (3.2)$$

with

$$\phi^{-1} = 1 + \left(\frac{\lambda}{2r}\right)^{-1} \quad (3.3)$$

$$K_i = \frac{2}{3}\sqrt{\frac{8RT}{\pi M_i}} \left[\text{m}^2/\text{s}\right] \quad (3.4)$$

The first term of the right side of Eq. (3.2) represents the contribution to Knudsen flow, the second the contribution to the slip flow at the wall and the third the viscous flow.

To describe the transport of gases in the porous anode the three parameters of the MTPM (Ψ, $\langle r \rangle$ and $\langle r^2 \rangle$) have to be determined experimentally. Diffusion and permeation experiments have been performed in order to determine textural properties of the cermet material. These experiments are described elsewhere [4]. The results are summarized in Table 1.

3. Reaction kinetics

Due to the fact that electrodes allowing a direct electrochemical oxidation of methane are nowadays not available the methane reforming within the anode-cermet is carried out in a two-stage step. The steam reforming of methane (IV) is thermodynamically favored at higher temperatures (it can be classified as strongly endothermic reaction) and lower pressures:

$$CH_4 + H_2O \underset{k_r^-}{\overset{k_r^+}{\rightleftarrows}} 3H_2 + CO \quad \Delta H_{298} = 206 \text{ kJ/mol} \quad \text{(IV)}$$

The electrochemically active fuels hydrogen and carbon monoxide are converted via shift reaction (V) into carbon dioxide and hydrogen.

$$CO + H_2O \underset{k_s^-}{\overset{k_s^+}{\rightleftarrows}} CO_2 + H_2 \quad \Delta H_{298} = -41 \text{ kJ/mol} \quad \text{(V)}$$

In spite of operating temperatures in the range of 750–900°C, it can be assumed that the shift reaction is very quick and remains in equilibrium. In order to describe the reforming kinetics in a simple way a quasi homogeneous expression of the kinetics is assumed. The rate expressions were determined experimentally [5]. The volumetric reaction rate of reaction (IV), expressed as moles of methane reacted per unit volume and time can be written as:

$$R_r = k_r^+ p_1 p_3 - k_r^- p_2 (p_4)^3 \left[\text{mol m}^{-3}\text{ s}^{-1}\right] \quad (4)$$

where k_r^+ and k_r^- denote the velocity constants of forward and backward steam reforming reaction. The shift reaction can be formulated with the velocity constants k_s^+ and k_s^- as:

$$R_s = k_s^+ p_2 p_3 - k_s^- p_4 p_5 \left[\text{mol m}^{-3}\text{s}^{-1}\right] \quad (5)$$

The velocity constants according to [5] are presented in Table 2.

Finally, the molar rates of formation can be formulated as follows:

$$R_{CH_4} = -R_r \left[\text{mol m}^{-3}\text{ s}^{-1}\right] \quad (6.1)$$

$$R_{CO} = R_r - R_s \quad (6.2)$$

$$R_{H_2O} = -R_r - R_s \quad (6.3)$$

$$R_{H_2} = 3R_r + R_s \quad (6.4)$$

$$R_{CO_2} = R_s \quad (6.5)$$

Due to the electrochemical reaction hydrogen and carbon monoxide will be consumed and water vapor and

Table 2
Velocity constants of steam reaction (k_r^+ and k_r^-) and shift reaction (k_s^+ and k_s^-) at different temperatures

Temperature (K)	k_r^+ (mol m^{-3} Pa^{-2} s^{-1})	k_r^- (mol m^{-3} Pa^{-4} s^{-1})	k_s^+ (mol m^{-3} Pa^{-2} s^{-1})	k_s^- (mol m^{-3} Pa^{-2} s^{-1})
1073	2.3×10^{-8}	1.4×10^{-20}	1.5×10^{-7}	1.4×10^{-7}
1123	8.0×10^{-8}	1.5×10^{-20}	3.2×10^{-7}	3.5×10^{-7}
1163	1.6×10^{-7}	1.5×10^{-20}	3.6×10^{-7}	4.3×10^{-7}

carbon dioxide will be produced, respectively. The electrochemical conversion of H_2 and CO takes place in the vicinity of the electrolyte/anode interphase. The depth of the reaction zone is about 50 μm. This is small compared to the 2 mm anode thickness and therefor the electrochemical reaction can be treated as a boundary condition in this model.

The conversion of hydrogen and carbon monoxide will be calculated according to the faraday law.

$$r = \frac{i_{H_2}}{2F} + \frac{i_{CO}}{2F} \left[\mathrm{mol\,m^{-2}\,s^{-1}}\right] \quad (7)$$

4. Results

4.1. Standard cermet

At the Research Centre Jülich the most experimental and theoretical investigations are carried out with the anode cermet ''NZ 40/2'' (for brevity referred to in the following just as standard cermet). That's the reason why the first simulations have been performed with its structural parameters (Table 1).

The boundary conditions for the simulation are as follows: the system is assumed to be isothermal with a temperature of 850°C. The pressure in the gas channel is 1 bar and the current density is 300 mA/cm^2. The inlet gas composition is assumed to be 30% pre-reformed methane (Table 3) and the thickness of the anode cermet is 2 mm.

The molar conversion rates R_i of the different components versus the depth of the anode is plotted in Fig. 2. According to the chemical reactions (IV and V), methane and steam are consumed and converted into hydrogen, carbon monoxide and carbon dioxide. A production is reflected by positive values of the molar rate of formation whereas a consumption is reflected by negative ones. Up to a cermet depth of 1.95 mm only the steam reforming reaction and the shift reaction dominate the total reaction rates of all gases. At the boundary of anode/electrolyte a conversion of carbon monoxide into carbon dioxide and of hydrogen into steam can be observed due to the electrochemical reaction.

4.2. Sensitivity analysis

It is the goal of the following sensitivity analysis to determine those structural parameters of the cermet that affect the methane conversion rate related to the geometric surface of the anode mostly. For each simulation, all structural parameters of the standard cermet and all base case operating conditions are set to be constant except the parameter being modified.

Fig. 3 shows the methane concentration inside the cermet for different values of ψ. In the gas channel the concentration of methane is the same in all three cases shown in the plot. Inside the cermet, a difference in the methane concentrations can be observed. A low value of ψ results in low methane concentrations, e.g., a reduction of

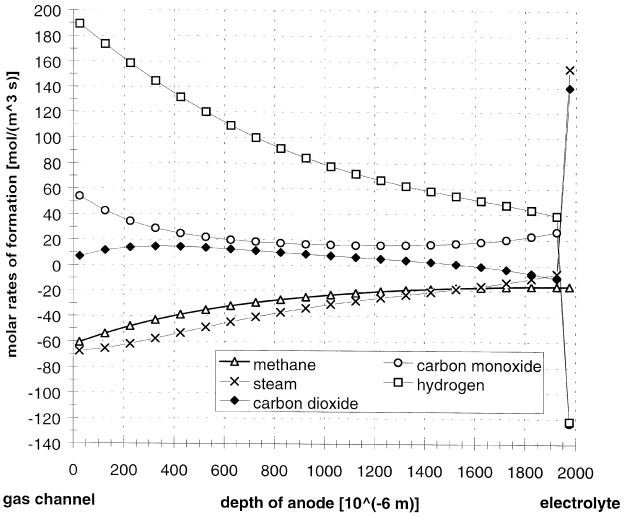

Fig. 2. Molar rates of formation at different positions inside the cermet: $T = 1123$ K, $i = 300$ mA/cm^2, standard cermet, 30% pre-reformed natural gas, normal pressure.

Table 3
Fuel composition after 30% pre-reforming of natural gas

Component	CH_4	CO	H_2O	H_2	CO_2
Molar fraction y (–)	0.171	0.029	0.493	0.263	0.044

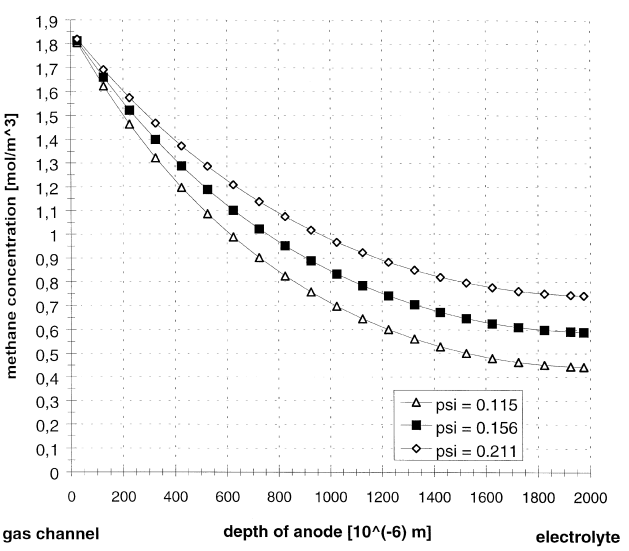

Fig. 3. Methane concentration at different positions inside the cermet for different ratios ψ: $T = 1123$ K, $i = 300$ mA/cm^2, $\langle r \rangle = 1.07 \times 10^{-6}$ m, $\langle r^2 \rangle = 3.8 \times 10^{-13}$ m^2, 30% pre-reformed natural gas, normal pressure.

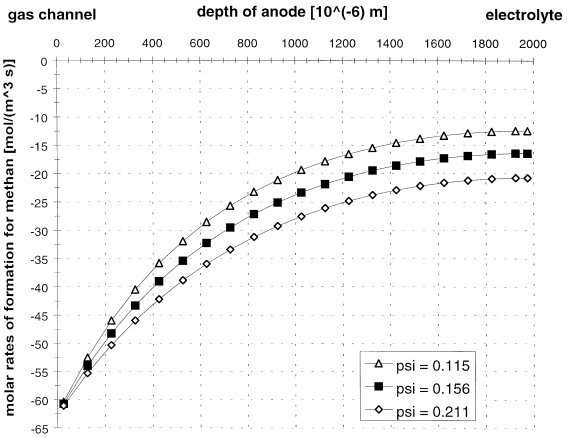

Fig. 4. Molar rate of formation for methane at different positions inside the cermet for different ratios ψ: $T = 1123$ K, $i = 300$ mA/cm^2, $\langle r \rangle = 1.07 \times 10^{-6}$ m, $\langle r^2 \rangle = 3.8 \times 10^{-13}$ m^2, 30% pre-reformed natural gas, normal pressure.

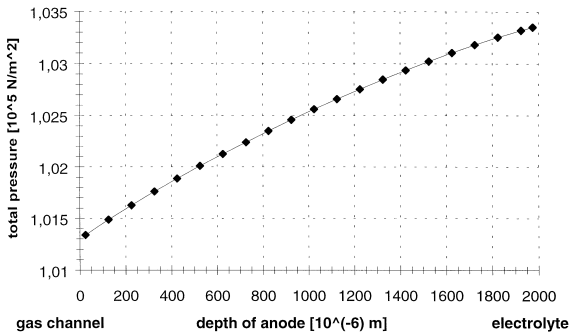

Fig. 5. Total pressure inside the anode: $T = 1123$ K, $i = 300$ mA/cm^2, standard cermet, 30% pre-reformed natural gas.

ψ from 0.211 to 0.115 increases the methane concentration from 0.82 mol/m^3 to 0.53 mol/m^3 at a distance of 1.425 mm from the surface. In Fig. 4, it can be seen that a decreasing of the value of ψ also decreases the methane conversion rate. Thus, by comparison of Fig. 3 with Fig. 4, it can be concluded that a lowering of ψ causes a lower overall methane conversion due to gas transport limitations in the cermet. This leads to the desired effect of a total methane conversion reduction. The data listed in Table 4 clearly show that in comparison to the standard cermet a reduction of ψ from 0.156 to 0.115 results in a lowering of the total molar methane conversion from -0.0572 mol/(m^2 s) to -0.0502 mol/(m^2 s). Moreover it is obvious that an increase in ψ corresponds with an increase in the total conversion.

Indeed a sensitivity analysis of all structural parameters ψ, $\langle r \rangle$ and $\langle r^2 \rangle$ show that ψ affects mostly the total molar methane conversion. It has to be stressed that a variation ψ by -26.28% relating to the data of the standard cermet affects the total conversion of methane in a way that its value decreases by 12.24%. The influence of the second structural parameter $\langle r \rangle$ has less effect on lowering the methane conversion. A reduction of -51.68% corresponds to a change in conversion rate of -10.14%. Finally, the results clearly show that no significant change in the methane conversion is achieved when the third parameter $\langle r^2 \rangle$ is varied.

In contrast to the first and second parameter a reduction of $\langle r^2 \rangle$ leads not to the desired reduction of the conversion rate but to a slight increase. This observation can be illuminated by the fact that the permeation flux of methane (in direction to the gas channel) is lowered and so more methane remains within the cermet. The reason of this contradiction to diffusion fluxes can be derived from Fig. 5. Because of the internal methane reactions the total pressure within the cermet increases with increasing cermet thickness, permeation fluxes must be noticed in direction to the gas channel.

4.3. Testing of produced cermets

In order to achieve conversion data of already produced cermets their structural parameters as summarized in Table 5 are implemented in each simulation run. The operating conditions remain constant ($T = 1123$ K, $i = 300$ mA/m^2) and as base case the standard cermet is considered, too.

Table 4
Results of the sensitivity analysis in view of a total methane conversion reduction. Two parameters have been fixed to the values of the standard cermet (see Table 5), the third parameter has been varied

Structural parameter	Value of the specific parameter	Variation compared to standard cermet (%)	Total conversion of methane [(10^{-2} mol/(m^2 s)]	Deviation compared to standard cermet (%)
ψ (–)	0.115	−26.28	−5.02	−12.24
	0.211	+35.26	−6.45	+12.76
$\langle r \rangle$ (10^{-6} m)	0.517	−51.68	−5.14	−10.14
	2.02	+88.79	−6.03	+5.42
$\langle r^2 \rangle$ (10^{-13} m^2)	1.8	−52.6	−5.72	+0.09
	15.3	+302.6	−5.7	−0.033

Table 5
Structural parameters and total methane conversion for different cermets: $T = 1123$ K, $i = 300$ mA/cm^2, 30% pre-reformed natural gas, normal pressure

Structural parameter	DS 42	Standard cermet	DS 45
ψ (–)	0.115	0.156	0.211
$\langle r \rangle$ (10^{-6} m)	0.517	1.07	2.02
$\langle r^2 \rangle$ (10^{-12} m^2)	0.18	0.38	1.53
Total methane conversion [10^{-2} mol/(m^2·s)]	−4.49	−5.72	−6.77
Conversion deviation (%)	−21.5	–	+18.36

The cermet called DS 42 has in comparison to the standard cermet a more fine porous structure and accordingly the total methane conversion is lowered by −21.5% to −0.0449 mol/(m^s s). A cermet with a more open porous structure leads to increasing conversions as can be seen by the cermet DS 45. Its total methane conversion increases to −0.0677 mol/(m^s s), a plus of 18.36%.

5. Conclusions

The present results demonstrate that among the structural parameters of a cermet which can be determined experimentally the ratio ψ is the one that affects the methane conversion mostly. The second parameter, the mean value of pore radii $\langle r \rangle$ should be considered as well. A reduction lead to a significant lowering of the these parameters' methane conversion, e.g., a ψ-reduction by −26.28% results in a methane conversion reduction by −12.24%. Considering already produced cermets it is found that in comparison with the standard cermet the total methane conversion can be lowered by −21.5% to −0.0449 mol/(m^2 s) while using the fine porous cermet DS 42.

6. List of symbols

B	Effective permeability coefficient	m^2 s^{-1}
c	Molar concentration	mol m^{-3}
D^m	Effective molecular diffusivity	m^2 s^{-1}
D^k	Effective Knudsen diffusivity	m^2 s^{-1}
ΔH	Enthalpy	J mol^{-1}
i	Current density	A m^{-2}
K	Knudsen number	–
k_r^+	Velocity constant of steam reforming (forward)	mol m^{-3} Pa^{-2} s^{-1}
k_r^-	Velocity constant of steam reforming (backward)	mol m^{-3} Pa^{-4} s^{-1}
k_s^+	Velocity constant of shift reaction (forward)	mol m^{-3} Pa^{-2} s^{-1}
k_s^-	Velocity constant of shift reaction (backward)	mol m^{-3} Pa^{-2} s^{-1}
N	Net molar flux density	mol m^{-2} s
p	Pressure	Pa
$\langle r \rangle$	Mean transport pore radius	m
$\langle r^2 \rangle$	Mean of squared transport pore radii	m^2
$\dot{r}$	Reaction rate	mol m^{-2} s^{-1}
R	Molar rate of formation	mol m^{-3} s^{-1}
t	Time	s
T	Temperature	K
x	Length coordinate	m
y	Mole fraction	–

Greek symbols

δ	Tortuosity	
ε	Porosity	
λ	Mean free path length	m
ψ	Ratio of porosity to tortuosity	–

Indices

d	Diffusion
i, j	Component
r	Steam reforming reaction
s	Shift reaction
z	Cell
x	Vector
$\underline{\underline{x}}$	Matrix

Constants

F	Faraday constant	9.648456×10^{-4} A s mol^{-1}
R_g	Gas constant	8.3144 J mol^{-1} K^{-1}

Acknowledgements

The authors like to thank K. Strauß for many useful discussions and the critical reading of the manuscript. Special thanks to the Max Buchner Forschungsstiftung for supporting this work.

References

[1] J. Meusinger, E. Riensche, U. Stimming, Reforming of natural gas in solid oxide fuel cell systems, J. Power Sources 71 (1998) 315–320.

[2] E. Achenbach, E. Riensche, Methane/steam reforming kinetics for solid oxide fuel cells, J. Power Sources 52 (1994) 283–288.
[3] D. Arnost, P. Schneider, Dynamic transport of multicomponent mixtures of gases in porous solids, Chem. Eng. J. 57 (1995) 91–99.
[4] J. Divisek, D. Froning, W. Lehnert, J. Meusinger, U. Stimming, Transport processes and methane reforming reactions in the SOFC-cermet anodes, IEA, 10th SOFC Workshop, Vol. 1, Les Diableret, Switzerland, 1997.
[5] Drescher, W. Lehnert, J. Meusinger, Structural properties of SOFC anodes and reactivity, Electrochim. acta 43 (1998) 3059–3068.